NeuroImage: Clinical 15 (2017) 151–160

Contents lists available at ScienceDirect

NeuroImage: Clinical

journal homepage: www.elsevier.com/locate/ynicl

Subtle alterations in cerebrovascular reactivity in mild cognitive impairment detected by graph theoretical analysis and not by the standard approach

Carlos A. Sánchez-Catasús[a,b,*], Gretel Sanabria-Diaz[c,d], Antoon Willemsen[a], Eduardo Martinez-Montes[d], Juan Samper-Noa[d,e], Angel Aguila-Ruiz[b], Ronald Boellaard[a], Peter P. De Deyn[f], Rudi A.J.O. Dierckx[a], Lester Melie-Garcia[c,d]

[a] Department of Nuclear Medicine and Molecular Imaging, University of Groningen, University Medical Center Groningen, The Netherlands
[b] Department of Nuclear Medicine, Center for Neurological Restoration (CIREN), Havana, Cuba
[c] Laboratoire de Recherche en Neuroimagerie (LREN), Centre Hospitalier Universitaire Vaudois (CHUV), Lausanne, Switzerland
[d] Neuroinformatics Department, Cuban Neuroscience Center, Havana, Cuba
[e] Hospital Carlos J. Finlay, Havana, Cuba
[f] Department of Neurology and Alzheimer Research Center, University of Groningen, University Medical Center Groningen, The Netherlands

ARTICLE INFO

Keywords:
Graph theoretical
Cerebrovascular reactivity
Mild cognitive impairment

ABSTRACT

There is growing support that cerebrovascular reactivity (CVR) in response to a vasodilatory challenge, also defined as the cerebrovascular reserve, is reduced in Alzheimer's disease dementia. However, this is less clear in patients with mild cognitive impairment (MCI). The current standard analysis may not reflect subtle abnormalities in CVR. In this study, we aimed to investigate vasodilatory-induced changes in the topology of the cerebral blood flow correlation (CBF_{corr}) network to study possible network-related CVR abnormalities in MCI. For this purpose, four CBF_{corr} networks were constructed: two using CBF SPECT data at baseline and under the vasodilatory challenge of acetazolamide (ACZ), obtained from a group of 26 MCI patients; and two equivalent networks from a group of 26 matched cognitively normal controls. The mean strength of association (*SA*) and clustering coefficient (*C*) were used to evaluate ACZ-induced changes on the topology of CBF_{corr} networks. We found that cognitively normal adults and MCI patients show different patterns of *C* and *SA* changes. The observed differences included the medial prefrontal cortices and inferior parietal lobe, which represent areas involved in MCI's cognitive dysfunction. In contrast, no substantial differences were detected by standard CVR analysis. These results suggest that graph theoretical analysis of ACZ-induced changes in the topology of the CBF_{corr} networks allows the identification of subtle network-related CVR alterations in MCI, which couldn't be detected by the standard approach.

1. Introduction

There is increasing evidence that patients with Alzheimer's disease (AD) dementia have decreased cerebrovascular reactivity (CVR) in response to a vasodilatory challenge, also defined as the cerebrovascular reserve (Glodzik et al., 2013, for a review). However, this is less clear in patients during the prodromal mild cognitive impairment (MCI) stage of AD. Some studies show a decrease (Richiardi et al., 2014; Glodzik et al., 2011; Cantin et al., 2011; Zavoreo et al., 2010), while others do not (Shim et al., 2015; Fromm et al., 2013; Anzola et al., 2011). This issue is becoming important in AD research because it could have implications for early diagnosis and treatment of AD. Early CVR abnormalities, especially at the microvascular level, affect the neurovascular coupling and consequently the neural activation (Pillai and Mikulis, 2015), which in turn alters the brain's functional integrity (Iadecola, 2004).

MCI due to AD is the transition from normal cognition to dementia (Albert et al., 2011). Accordingly, CVR abnormalities would be subtle or borderline which may partly explain ambiguous findings, particularly in MCI patients with a low vascular burden. Furthermore, considering the complexity of the cerebral microvasculature network the standard analysis of CVR might not reflect subtle network-related alterations since it relies on the analysis of individual regions (or the whole brain) rather than on the interaction between them.

Recently, graph theoretical analysis of large-scale structural MRI (sMRI) correlation networks has shown its potential to reveal subtle network-related pathological processes in MCI (Tijms et al., 2013; He et al., 2009a, for reviews). We previously demonstrated that the

* Corresponding author at: University Medical Center Groningen, Department of Nuclear Medicine and Molecular Imaging. Hanzeplein 1, 9713 GZ Groningen, The Netherlands.
E-mail address: c.a.sanchez.catasus@umcg.nl (C.A. Sánchez-Catasús).

http://dx.doi.org/10.1016/j.nicl.2017.04.019
Received 1 September 2016; Received in revised form 10 March 2017; Accepted 19 April 2017
Available online 25 April 2017

cerebral blood flow correlation (CBF_{corr}) network, based on CBF SPECT data, shows a non-random topological organization (Melie-García et al., 2013). The same topological organization had been previously observed in sMRI correlation (Alexander-Bloch et al., 2013, for a review) and fiber tractography networks (Iturria-Medina et al., 2008). Therefore, we speculate that graph theoretical analysis can also be applied to CBF SPECT data to detect possible subtle network-related CVR abnormalities in MCI.

Here, we constructed four CBF_{corr} networks: two using CBF SPECT data at baseline and under the vasodilatory challenge of acetazolamide (ACZ), obtained from a group of relatively young MCI patients with limited vascular risk factors; and two equivalent networks using a group of matched cognitive normal controls. ACZ is a reproducible, simple, and a safe vasodilatory stimulus (Vagal et al., 2009, for a review).

Graph metrics based on the concepts of the mean strength of association (*SA*) (Bullmore and Bassett, 2011) and clustering coefficient (*C*) (Watts and Strogatz, 1998) were used to evaluate ACZ-induced changes on the topology of the CBF_{corr} networks. The *SA* for a particular brain region (node) measures the correlation's mean (co-variation's mean) with the rest of the network; while *C* measures local connectivity (i.e. how well neighbors of a node are connected).

Hence, using graph theoretical analysis, our aim was to investigate ACZ-induced changes in the topology of the CBF_{corr} network to study possible network-related CVR abnormalities in MCI. We also investigated CVR by the standard approach in the same groups of subjects for comparing with graph theoretical analysis findings.

2. Methods

2.1. Subjects

Twenty-six MCI patients and twenty-six clinically healthy control volunteers were studied, selected from one hundred subjects recruited over a two-year period and a one-year follow-up and based on the inclusion and exclusion criteria detailed below. The Ethics Committee of the Center for Neurological Restoration of Havana, Cuba, approved the study. All participating subjects gave written informed consent according to the Helsinki Declaration. Table 1 summarizes sociodemographic and clinical characteristics of the MCI and control groups.

All subjects were screened for a complete medical history, routine blood tests, cranial MRI, neuropsychological testing and neurological/psychiatric examinations. Subjects were clinically diagnosed as MCI using the criteria based on the Clinical Dementia Rating Scale (CDR) (Morris, 1993). According to these criteria, subjects were classified as MCI with CDR = 0.5; while normal cognitive subjects with CDR = 0. All of MCI subjects maintained independence in their daily living. In addition to the Mini-Mental State Examination (MMSE), specific mnemonic and non-mnemonic cognitive tests were also performed for all subjects to further characterize cognitive function (Supplementary Table S1).

Table 1
Sociodemographic and clinical features of control and MCI groups.

	Control (N = 26)	MCI (N = 26)	p-value
Age (years)	60.9 ± 7.3	64.7 ± 6.9	0.06[a]
Gender (female/male)	13/13	14/12	0.78[b]
Education (years)	13.6 ± 3.9	11.8 ± 4.6	0.13[a]
MMSE	29.3 ± 1.1	26.9 ± 1.24	10^{-6}[a]
Hypertension	27%	35%	0.55[b]
Hyperlipidemia	19%	23%	0.73[b]
Diabetes	15%	15%	1[b]
Smoking	27%	19%	0.51[b]

Data shown as mean ± SD or percent of subjects.
[a] Student *t*-tests for independent samples.
[b] Chi-square test.

The inclusion criteria were: 1) MCI patients with memory complaints as the main cognitive symptom, which worsened over a period of one year; 2) subjects (patients and controls) with limited (and treated) vascular risk factors, based upon clinical examination, blood tests and magnetic resonance angiography (MRA) findings; 3) subjects without significant depression, according to the Hamilton Depression Scale (score < 8) (Hamilton, 1960); 4) no prior or current treatment with anti-acetylcholinesterase agents; and 5) right-handedness.

The exclusion criteria were: 1) significant medical problems (i.e. serious cardiac disease, poorly controlled diabetes or hypertension; severe inflammatory, thyroid, renal, hepatic or other chronic diseases); 2) cerebrovascular disorders (i.e. transient ischemic attack or cerebral infarction), moderate and severe carotid stenosis by MRA findings, large white matter changes on MRI (based on T2 and FLAIR sequences), hydrocephalus or intracranial mass; 3) history of traumatic brain injury, migraine or another neurological disease; and 4) psychiatric disorder, substance abuse or dependence.

2.2. CBF SPECT imaging under the acetazolamide challenge

CBF SPECT imaging was carried out by a double-head rectangular gamma camera (Sopha Medical Vision, France) equipped with ultra-high-resolution fan beam collimators. More about the acquisition and reconstruction parameters, including corrections for attenuation and partial volume effect (PVE) due to atrophy, are described in our preceding article (Melie-García et al., 2013). A two-day protocol was used for CBF SPECT imaging at baseline (basal SPECT) and under the ACZ challenge (ACZ SPECT).

Absolute measurement is necessary to quantify (optimally) the CBF response to the vasodilatory stimulus (Boles Ponto et al., 2004). Therefore, global CBF at basal condition ($gCBF_{Basal}$) and under ACZ ($gCBF_{ACZ}$) was determined in absolute units (mL/min/100 g) by spectral analysis of non-invasive radionuclide angiographies (Takasawa et al., 2002). The radionuclide angiography was performed before SPECT acquisition, for both basal and ACZ conditions. Briefly, a radionuclide angiography of the head and chest was performed after injection of 555 MBq of technetium-99-ethyl cysteinate dimer (ECD) into the antecubital vein of the right arm under resting condition (supine, eyes open, dimly lit quiet room) to estimate $gCBF_{Basal.}$ The same procedure was repeated to estimate $gCBF_{ACZ}$ but 20 min after slow intravenous injection of 1 g of ACZ. Heart rate and arterial pressure were measured at the time of the two injections of the tracer (basal and ACZ).

Basal and ACZ SPECT images were then converted to basal and ACZ quantitative CBF images using $gCBF_{Basal}$ and $gCBF_{ACZ}$, respectively, by application of Lassen's linearization algorithm (Lassen et al., 1988). For subsequent voxelwise statistical analysis, basal and ACZ quantitative CBF images were normalized to the Montreal Neurological Institute (MNI) space. The image normalization was performed by applying DARTEL parameters (based on a fast diffeomorphic algorithm) obtained from MRI preprocessing (see the next subsection). Normalized images were then smoothed using a 14 mm-kernel to optimize sensitivity (Van Laere et al., 2002).

2.3. Volumetric MRI

Volumetric high-resolution MRI was also performed to characterize the MCI group regarding regional brain atrophy. Regional atrophy, particularly hippocampal, is a biomarker of neuronal injury of MCI due to AD (Albert et al., 2011; Sánchez-Catasús et al., 2017). Volumetric MRI also had two other functions: to correct for PVE in CBF SPECT images and to estimate spatial transformations that were used to normalize images to MNI space, as described above.

MRI acquisition was performed using a 1.5 Tesla Symphony scanner (Siemens, Erlangen, Germany). The acquisition protocol for volumetric MRI is described in details in our previous study (Melie-García et al.,

2013). The preprocessing steps were as follows: images were segmented into GM and WM; imported into the DARTEL toolbox and normalized to MNI space to generate warped and smoothed (12 mm-kernel) Jacobian modulated GM and WM images. GM/WM modulated images represent GM/WM volume images (GMV/WMV images). Global tissue volumes were estimated in the native space using the Voxel-Based Morphometry toolbox (VBM8: http://dbm.neuro.uni-jena.de/vbm8/).

For every subject, neurological/psychiatric/neuropsychological examinations, as well as SPECT and MRI, were carried out within a maximum interval of one month.

2.4. Construction of the CBF correlation (CBF_{corr}) network

For each group of subjects (MCI and control) in each condition (baseline and ACZ challenge), a CBF_{corr} network was constructed as a CBF correlation matrix (Melie-García et al., 2013). In short, 90 ROIs were defined using the AAL atlas (Tzourio-Mazoyer et al., 2002) and Pearson's correlation coefficients were calculated (across subjects) between all possible pairs of ROIs. Hence, the interregional correlation matrix (90 × 90 ROIs) was obtained gathering together all correlation coefficients. Self-correlations were excluded, implying a diagonal of zeros in the symmetric matrix. Prior to the correlation analysis, a linear regression was performed at every ROI to remove the effects of age, gender, age–gender interaction, and global CBF values. For computing the CBF correlation matrix, the correlation was carried out between the residuals of this regression instead of the raw regional CBF values. Fig. 1 shows CBF correlation matrices for each group in each condition.

For within-conditions and within-groups network metrics comparisons (see Sub-section 2.6.2), we obtained 1000 bootstrap samples (with replacement) of each CBF correlation matrix. Paired bootstrap samples were used for baseline and the ACZ challenge in each group.

2.5. Network metrics

In the following, we define *SA* (the mean strength of association) (Bullmore and Bassett, 2011) and *C* (the clustering coefficient) (Watts and Strogatz, 1998) to study ACZ-induced changes in the CBF correlation networks.

The *SA* for a particular brain region or node *i*, SA_{nodal} (*i*), is defined as the mean of the absolute value of Pearson's correlation coefficients ($Corr_{ij}$) of node *i* with the rest *N*-1 nodes in the network. Formally, SA_{nodal} (*i*) is calculated as:

$$SA_{nodal}(i) = \frac{1}{N-1} \sum_{\substack{j=1 \\ j \neq i}}^{N} |Corr_{ij}|$$

where *N* is the number of nodes (ROIs).

In simple terms, SA_{nodal} measures the correlation's mean (covariation's mean) of a node with the rest of the network. *SA* is also defined at the network level (SA_{global}) as the average of SA_{nodal}:

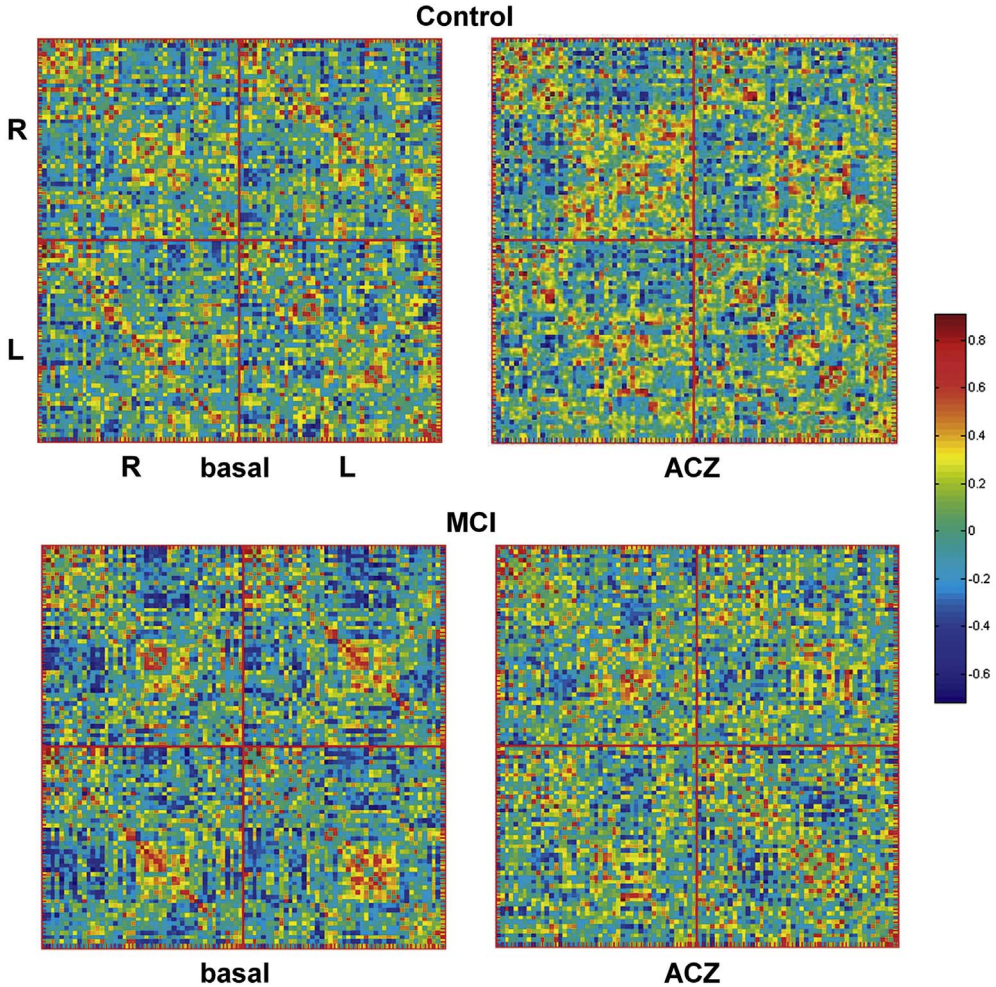

Fig. 1. CBF correlation matrices (CBF correlation networks) constructed using CBF SPECT data at basal and under the acetazolamide (ACZ) challenge for MCI and cognitively normal controls. The color bar indicates the value of the correlation coefficient coming from the CBF co-variations among 90 anatomical brain regions (AAL atlas). For the sake of clarity brain regions of the right (R) and left (L) hemispheres were separated.

$$SA_{global} = \frac{1}{N} \sum_{i=1}^{N} SA_{nodal}(i)$$

On the other hand, C is a measure of the tendency to cluster nodes into strictly connected neighborhoods (a measure of network segregation; i.e. local connectivity). Nodes are considered neighbors when a connection between them exists, which is not limited to a physical neighborhood concept. C_{nodal} (i), for a binary and undirected graph G, is the number of existing connections between the neighbors of node i divided by all neighbor's possible connections. Formally, C_{nodal} (i) is calculated as:

$$C_{nodal}(i) = \frac{1}{N} \sum_{i \in G} \frac{2t_i}{k_i (k_i - 1)}$$

where t_i is the number of triangles around node i (see below); and k_i is the degree of node i (number of links connected to node i); (for $k_i < 2$, C_{nodal} $(i) = 0$).

$$t_i = \frac{1}{2} \sum_{j,h \in G} a_{ij} a_{ih} a_{jh}$$

where a_{ij} is the connection status between i and j: $a_{ij} = 1$ when link (i, j) exists (when i and j are neighbors); $a_{ij} = 0$ otherwise ($a_{ii} = 0$ for all i).

In simple terms, C_{nodal} measures how well neighbors of a node are connected. C is also defined at the network level (C_{global}) as the average of C_{nodal}:

$$C_{global} = \frac{1}{N} \sum_{i=1}^{N} C_{nodal}(i)$$

For each CBF correlation matrix, SA_{nodal} and SA_{global} were calculated over the bootstrap samples. Since we used C defined for a binary (undirected) graph, C_{nodal} and C_{global} were calculated over bootstrap samples of thresholded binary adjacency matrices. Rather than restricting the analysis to a binary graph obtained by applying a single threshold value, C_{nodal} and C_{global} were calculated over a range of thresholds or 'sparsity degree' values. A sparsity degree of 0.9 means that 90% of the correlation matrix is discarded; consequently, only the highest 10% of the values is taken into account. Sparsity degrees ranging from 0.5 to 0.9 (in steps of 0.02) were used, yielding a set of 21 values. This procedure normalizes the networks to have the same number of nodes and edges, enabling the examination of C_{nodal} and C_{global}. The range of sparsity degree was chosen to allow for these network properties to be estimated and the number of spurious edges in each network minimized as indicated in previous studies (Achard and Bullmore, 2007; He et al., 2007; Sanabria-Diaz et al., 2013).

Before calculating C_{nodal} (as described above), the largest connected component (see Achard et al., 2006) of all bootstrap samples of CBF correlation matrices was computed. The minimum sparsity degree for the largest connected component (equal to the number of AAL nodes) was used as the upper limit of the sparsity degree range. This step guarantees that all C_{nodal} values come from fully connected CBF_{corr} networks. Then, the C_{nodal} mean curve (across the range of sparsity degree) was assessed over the bootstrap samples for every node and used as the C_{nodal} descriptor.

On the other hand, the descriptor used for C_{global} was the area under the curve (AUC) extracted from thresholding across the range of sparsity degree over bootstrap samples for each group and condition. Since the topology of the C_{global} curve is monotonic with the sparsity degree, the AUC is a suitable descriptor for characterizing its global performance. This descriptor was also adopted in previous studies (Sanabria-Diaz et al., 2013; Wu et al., 2012; He et al., 2009b).

Construction of CBF_{corr} networks and computation of network metrics was performed using the MorphoConnect toolbox (Melie-García et al., 2010) and subroutines of the Brain Connectivity toolbox (https://sites.google.com/site/bctnet/).

2.6. Statistical analysis

2.6.1. Changes in standard metrics

The data at the voxel level was analyzed by a 2 (group: Control and MCI) × 2 (condition: basal and ACZ) full factorial design as implemented in the SPM8 toolbox. Age and gender were modeled as nuisance covariates. The global effect was also controlled using proportional scaling.

We examined simple main effects of condition (positive and negative) in each group by t-contrasts for dependent samples; and simple main effects of group (positive and negative) in each condition by t-contrasts for independent samples. We also studied the interaction of group and condition (positive and negative).

A similar treatment (2 × 2 design) was also performed for global CBF values, controlling for age and gender.

As a supplementary morphometric analysis, differences at the voxel level between groups for GMV and WMV images were tested to evaluate regional brain atrophy in the MCI group. Comparisons were performed using the Student t-tests for independent samples through the SPM8 toolbox. The GMV and WMV images were masked using an absolute threshold of 0.25 to avoid as much as possible contamination by misclassified voxels. Age, gender, and total intracranial volume were controlled.

In all SPM analyses, the statistical threshold of $p = 0.01$ (peak level) was used. The extent threshold used was determined by the cluster of voxels significant at $p = 0.05$ (cluster level), corrected for multiple comparisons (family-wise error method - FWE) and after correction of non-isotropic smoothness. Anatomical regions were determined by comparing voxel and cluster location with the AAL atlas (Tzourio-Mazoyer et al., 2002). The most significant voxels were reported in MNI coordinates.

2.6.2. Changes in network metrics

Similar to the standard analysis, C and SA (global and nodal) were analyzed by a 2 × 2 design. To examine simple main effects of the condition in each group for each network metric (or simple main effects of the group in each condition), we computed the difference between the two conditions (or between the two groups) for the corresponding bootstrap samples. Then, we constructed the bootstrap distribution of the difference and computed the 95% BC (bias-corrected) bootstrap confidence interval (CI). A significant difference between conditions (or between groups) was considered when the CI did not contain the zero. For C_{nodal} and SA_{nodal}, we also corrected for multiple comparisons by Bonferroni adjustment.

Likewise, we studied the interaction of group and condition (global and nodal) by comparing simple main effects of condition between groups following the same procedure as described in the previous paragraph. For instance, the differences between conditions in control and MCI groups were subtracted and the 95% BC bootstrap CI was calculated for the subtraction. As before, if CI did not contain the zero, the interaction effect was considered statistically significant. Due to the exploratory nature of this study, we also examined the interaction for uncorrected values at the nodal level.

The network statistical analyses were performed using the MorphoConnect toolbox (Melie-García et al., 2010), while global CBF data was analyzed using STATISTICA software (Stat Soft, Inc., version 8.0). The significance level was set at $p < 0.05$.

3. Results

The administration of ACZ was well tolerated in all individuals. There were no significant differences between conditions (basal vs. ACZ) in both groups in heart rate (Control: 68.2 ± 9.9 vs. 67.2 ± 9.4 bpm, respectively, $p = 0.6$, paired t-test; MCI: 70.4 ± 9.4 vs. 67.4 ± 7.1 bpm, respectively, $p = 0.09$) and mean arterial pressure (Control: 106.9 ± 10.8 vs. 106.5 ± 9.9 mm Hg,

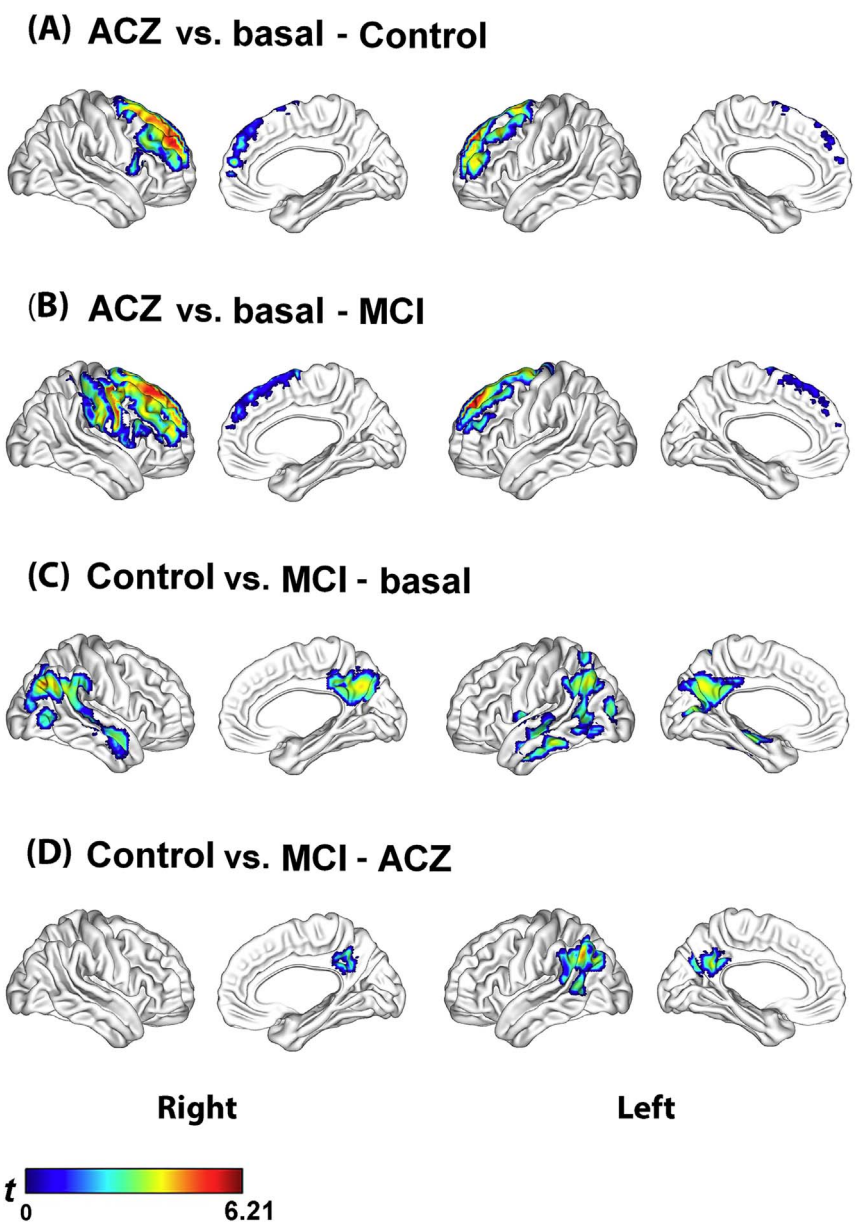

Fig. 2. CBF changes at the voxel level analyzed by a 2 (group: Control and MCI) × 2 (condition: basal and ACZ) full factorial design using statistical parametric mapping (SPM). Figures A and B show that the control and MCI groups had a similar regional pattern of CBF increase in frontal lobe bilaterally. Figures C and D show that the regional differences between groups were relatively similar in the two conditions, although less extensive in the ACZ condition. No interaction of the group by the condition was found.
SPM t-maps are visualized onto the cortical surfaces using the BrainNet Viewer package (http://www.nitrc.org/projects/bnv).

respectively, p = 0.8; MCI: 102. 8 ± 10.9 vs. 105.9 ± 10.8 mm Hg, respectively, p = 0.1).

3.1. Changes in standard metrics

At the global level, there was a significant increase in $gCBF_{ACZ}$ as compared with $gCBF_{Basal}$ in both groups (Control: 42.0 ± 5.5 vs. 54.9 ± 6.3 mL/min/100 g; $p < 10^{-6}$; MCI: 38.9 ± 6.7 vs. 51.1 ± 7.3 mL/min/100 g; $p < 10^{-6}$) (Supplementary Fig. S1). The percent of the increase in the control group (+ 31.4 ± 9.2) was comparable to that found in the MCI group (+ 32.7 ± 12.9). There were no significant differences between groups in the basal (p = 0.21) and ACZ conditions (p = 0.07). No significant interaction of group and condition was found (p = 0.75).

At the voxel level, the analysis of differences between condition within-group showed a similar pattern in the control and MCI groups. Both groups showed significant regional CBF increases mainly in frontal regions bilaterally, after removal of the effect of global CBF increase due to ACZ (Fig. 2.A and B, Supplementary Table S2). In the control group, the voxel with the lowest p-value was found in the right superior frontal gyrus (medial part) (MNI: x, y, z = 15, 56, 31; $P_{FWE} = 10^{-3}$, T = 6.21). In the MCI group, the right superior frontal gyrus (dorsolateral part) was the voxel with the lowest p-value (MNI: x, y, z = 15, 35, 55; $P_{FWE} = 10^{-3}$, T = 6.18). Neither group showed a significant regional decrease.

On the other hand, the group difference within-condition showed a regional CBF decrease in the MCI group as compared to the control group in the basal condition, mostly in temporoparietal regions bilaterally (Fig. 2.C, Supplementary Table S3). In the right angular gyrus was the voxel with the lowest p-value (MNI: x, y, z = 45, −70, 34; $P_{FWE} = 0.05$, T = 4.52). At the ACZ condition, the results were relatively similar to those observed in basal condition, although less extensive and the right temporoparietal region showed no difference as compared to the control group (Fig. 2.D, Supplementary Table S3). In

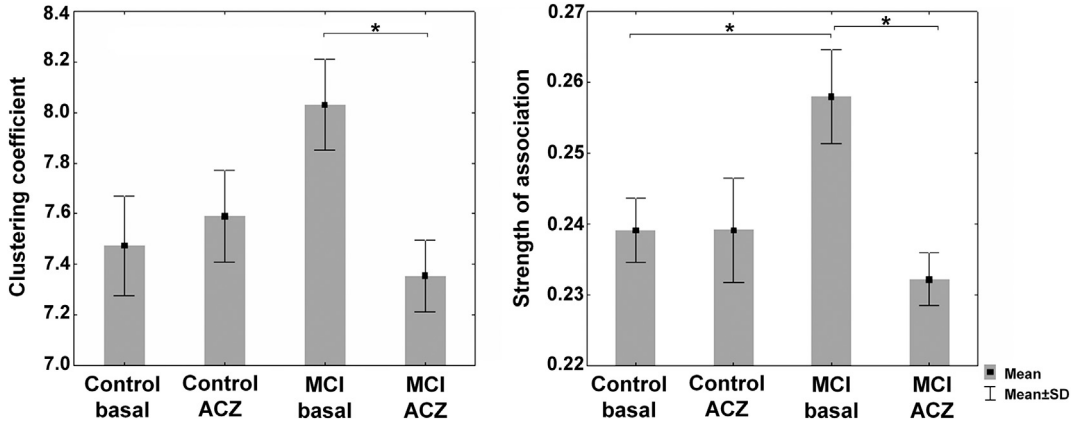

Fig. 3. Global clustering coefficient ($C_{globlal}$) and mean strength of association (SA_{global}) in the control and MCI groups in the two condition: basal and under the ACZ challenge. The data were generated by bootstrapping the CBF correlation matrices (1000 samples per group and condition). Comparisons were performed by estimating 95% bootstrap confident intervals (see main text for details). *Significant effect.

the left angular gyrus was the voxel with the lowest p-value (MNI: x, y, z = − 45, 61, 37; P_{FWE} = 0.004, T = 5.17). In the basal and ACZ conditions in the MCI group, as compared to the control group, also no significant regional CBF increases were found. No significant interaction of group and condition were observed neither positive nor negative.

3.2. Changes in network metrics

At the global level, the control group showed no significant changes of C_{global} and SA_{global} (no changes of CBF co-variation) in response to the ACZ challenge. In contrast to the control, the MCI group showed a decrease in $C_{globlal}$ and SA_{global} (Fig. 3 and Table 2; see also Supplementary Fig. S2).

Moreover, SA_{global} was higher in the MCI group as compared to the control in the basal condition (Fig. 3 and Table 2). Although not significant, a similar difference for $C_{globlal}$ in the MCI group was found (Fig. 3 and Supplementary Fig. S2). At the ACZ condition, no significant differences were observed for C_{global} and SA_{global} between the MCI and control groups (Fig. 3 and Table 2; see also Supplementary Fig. S2). However, unlike the standard analysis, we found a significant crossover interaction effect of group and condition for SA_{global} (Table 2). Thus, compared to the control group, the MCI group showed a specific decrease in SA_{global} induced by the ACZ challenge. For C_{global}, a similar interaction was observed although did not reach significance (Supplementary Fig. S2).

At the nodal level, the control group showed no significant change in C_{nodal} in response to ACZ after multiple comparisons correction (4.A and 4.B); while SA_{nodal} showed an increase in the right inferior temporal gyrus (Fig. 4.C) and decreases in the frontal superior and middle temporal pole on the left side (Fig. 4.D). In contrast to the control, the MCI group showed decreases in C_{nodal} in the hippocampus and the fusiform gyrus on the right side and in the dorsal medial prefrontal cortex on the left side (Fig. 4.E and F). In this group, SA_{nodal} increased in the postcentral gyrus (Fig. 4.G) and decreased in the superior frontal, middle frontal, lingual and fusiform gyri on the right side, and in the left middle occipital gyrus (Fig. 4.H).

On the other hand, the group difference within-conditions showed that in the MCI group, in the basal condition, C_{nodal} was increased in the inferior parietal lobe bilaterally and in lingual and fusiform gyri on the right side (Fig. 5.A and B); whereas SA_{nodal} was increased in the lingual gyrus bilaterally and in the right inferior temporal and left middle occipital gyri (Fig. 5.C and D). At the ACZ condition, both groups showed no significant changes in both C_{nodal} and SA_{nodal} (Fig. 5.E–H).

However, similar to global network metrics, there was a significant crossover interaction effect of group and condition for both C_{nodal} and SA_{nodal} (Fig. 6). Compared to the control group, the MCI group showed a specific decrease in C_{nodal} induced by the ACZ in the lingual, fusiform and superior temporal gyri on the right side after multiple comparisons correction (Fig. 6.A); and a specific decrease in SA_{nodal} in the middle frontal region and in the lingual, fusiform and inferior temporal gyri on the right side and in the left thalamus (Fig. 6.C).

When the interaction effects described above were examined less conservatively (uncorrected statistic), we found that the MCI group showed a specific decrease in C_{nodal} mainly in regions comprising the inferior parietal lobe and medial prefrontal cortex bilaterally, the parahippocampal gyrus and the lateral temporal cortex on the right side (Fig. 6.E and F). Both thalamus also showed a decrease in C_{nodal}. Moreover, a specific increase in C_{nodal} was found mainly in frontal and occipital regions on the right side, and in the anterior and posterior cingulate on the left side. Likewise, SA_{nodal} showed concurrent changes in C_{nodal} (increase or decrease) in several regions as shown in the Fig. 6.E–H. An opposite change in C_{nodal} and SA_{nodal} was also observed in the right middle frontal region (Fig. 6.E and G).

Table 2
Simple main effects and interactions of group and condition at the global level.

Effect	Mean (95% CI) - C_{global}	Mean (95% CI) - SA_{global}
ACZ vs. basal (Control)	0.12 (− 0.90 – + 0.63)	0.00004 (− 0.02 – + 0.009)
ACZ vs. basal (MCI)	− 0.68 (− 1.44 – − 0.97)[a]	− 0.026 (− 0.04 – − 0.01)[a]
Control vs. MCI (basal)	− 0.56 (− 1.28 – + 0.16)	− 0.019 (− 0.03 – − 0.003)[a]
Control vs. MCI (ACZ)	0.24 (− 0.61 – + 0.84)	0.007 (− 0.02 – + 0.02)
Interaction	0.79 (− 0.14 – + 1.75)	0.03 (+ 0.0006 – + 0.04)[a]

ACZ, acetazolamide; CI, confident interval.
[a] Significant effect.

3.3. Supplementary morphometric analysis

Regional GMV was decreased significantly in the lateral and medial temporal regions (including hippocampi) in the MCI group compared with the control group (Supplementary Fig. S3 and Supplementary Table S4). In contrast to GMV, no significant differences were observed between groups in WMV.

4. Discussion

This study investigated ACZ-induced changes in the topology of the CBF_{corr} networks in normal cognition and MCI subjects. We found that normal cognition and MCI show different patterns of *C* and *SA* changes,

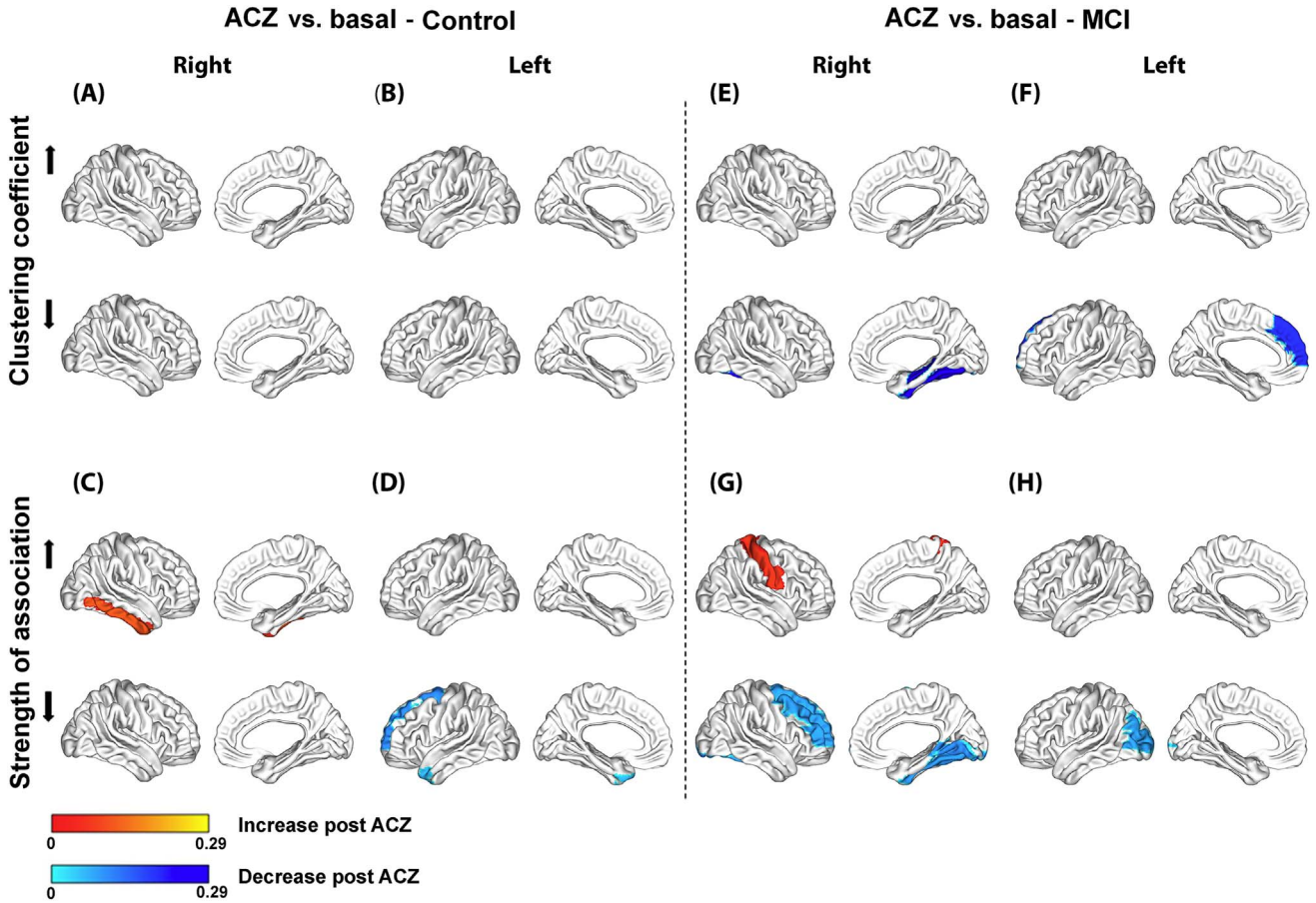

Fig. 4. Significant differences between condition within-group at the nodal level for the clustering coefficient (C_{nodal}) and mean strength of association (SA_{nodal}) in the control (A–D) and MCI groups (E–H).
Regional changes are mapped onto the cortical surfaces using the BrainNet Viewer package (http://www.nitrc.org/projects/bnv).

while the standard approach did not detect substantial differences. Thus, our findings support the concept that multivariate measures (i.e. co-variations) combined with a graph theoretical approach are more sensitive to identify complex pathological processes, as has found in other brain diseases (Bassett et al., 2012; He et al., 2009b). Univariate measures derived from the standard approach could be insufficient for capturing subtle (early) abnormal changes.

4.1. CBF imaging under the ACZ challenge

The global CBF increase in both groups verifies the reliability of the methodology used for CBF imaging under the ACZ challenge. The percent of the increase in the two groups was comparable to previous studies in healthy subjects using a similar methodology (Boles Ponto et al., 2004, for a review).

An interesting observation is the highest regional CBF increase in response to ACZ in frontal cortices in both groups (Fig. 2.A and B). As far as we know, this has not been previously reported. The highest frontal CBF is possibly caused by greater oxygen metabolism in these regions before ACZ administration. This explanation is substantiated by the fact that the neuronal activity is high in frontal regions during the resting state (Ingvar, 1979) and there is a direct relationship between the CBF response to the ACZ and pre-existing oxygen metabolic activity (Yamauchi et al., 2002).

Moreover, the basal temporoparietal CBF reduction observed in the MCI group as compared to the control group (Fig. 2.C) is the typical AD-like hypoperfusion pattern previously described (Herholz et al., 2002). The group difference in the ACZ condition was also relatively similar to those observed in the basal condition. Thus, the basal regional CBF reduction in the MCI group was not misery perfusion since microvessels responded to the ACZ. The basal hypoperfusion is likely mainly related to a reduced level of regional metabolic activity (Herholz et al., 2002).

4.2. Patterns of ACZ-induced changes in CBF correlation networks

The control (cognitively normal) group network showed only a little or almost no topological changes in response to the ACZ challenge (Figs. 3 and 4.A–D). That is, the control group network seems to have the capability to adapt to the challenge. Possibly, this reflects the process to maintain the brain microenvironment homeostasis (Iadecola, 2004), vital for brain function, in response to the vascular challenge induced by the ACZ (Vagal et al., 2009). In contrast, the MCI group network showed a decrease in C and SA, especially at the global level (Fig. 3), suggesting that the above process is possibly altered to some extent in the MCI stage not detected by the standard analysis. On the other hand, although speculative, the SA_{global} increase in the MCI group network in the basal condition might represent an adaptive mechanism in response to the effects of the pathological process.

Perhaps, the most revealing finding is the crossover interaction effect between group and condition, in particular, when analyzed in a less conservative way (Fig. 6.E–H). For example, the patterns of C_{nodal} and SA_{nodal} decreases (mainly C_{nodal}, the bottom of Fig. 6.E and F) partially correspond with the regional CBF reduction in the MCI group in the basal condition (Fig. 2.C). The overlap increases if the atrophy found in the MCI group is included (Supplementary Fig. S3), which suggests that these functional and structural abnormalities could be related to the ACZ-induced changes observed in the MCI group network since they are both biomarkers of neuronal injury of MCI due to AD

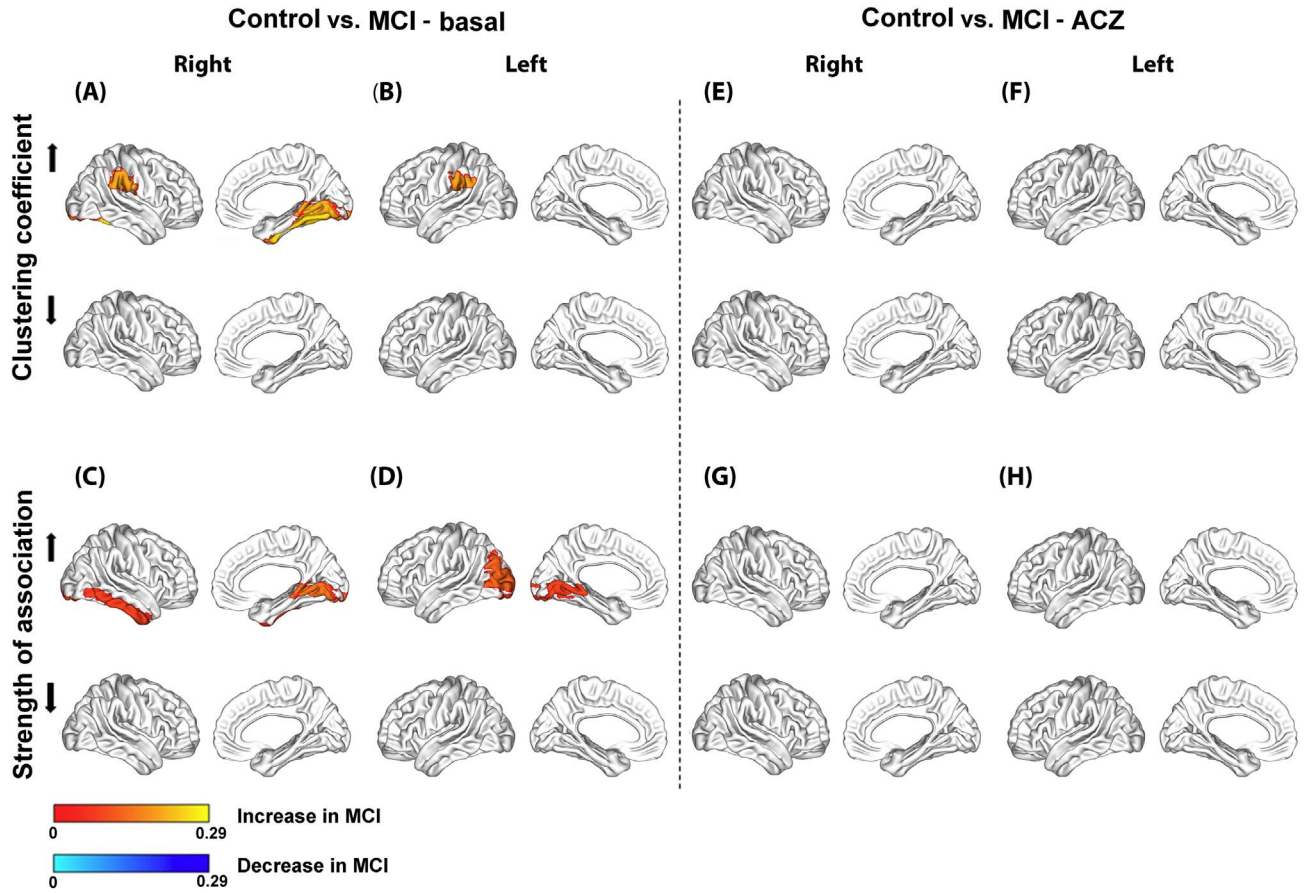

Fig. 5. Significant differences between group within-condition at the nodal level for the clustering coefficient (C_{nodal}) and mean strength of association (SA_{nodal}) in the basal (A–D) and ACZ conditions (E–H).
Regional changes are mapped onto the cortical surfaces using the BrainNet Viewer package (http://www.nitrc.org/projects/bnv).

(Sánchez-Catasús et al., 2017, for a review).

Interestingly, the patterns of C_{nodal} decrease (the bottom of Fig. 6.E and F) also overlap to a certain extent with the default mode network (DMN), which is very active in the resting state (Hafkemeijer et al., 2012, for a review). Thus, it is plausible that these patterns could be related to altered changes in the topology of the DMN's vascular component, considering that the CBF_{corr} network was studied in two resting states: pre-ACZ and under the effect of the ACZ. It is known that DMN also overlaps the brain network underlying the episodic memory (Rugg and Vilberg, 2013) that is specifically affected in MCI due to AD (Albert et al., 2011).

Furthermore, the DMN regions are also targets of the AD process (Ingelsson et al., 2004; Villain et al., 2012), which may disrupt CBF co-variation in response to the vasodilatory challenge. The available evidence suggests that various pathological mechanisms of AD may contribute to alterations of CVR as a result of damage to the cerebrovascular system (Glodzik et al., 2013, for a review). Nevertheless, such mechanisms could have less expression in the MCI stage, especially in patients with a low vascular load. Consequently, subtle CVR alterations would be difficult to detect by the standard approach, in agreement with previous studies with negative findings (Shim et al., 2015; Fromm et al., 2013; Anzola et al., 2011).

Moreover, the C_{nodal} increase in the MCI group network in the basal condition (the top of Fig. 5.A and B) also showed a partial correspondence with the C_{nodal} decrease induced by the ACZ (the bottom of Fig. 6.E and F). This overlap implies that in these regions C_{nodal} is changing from a high basal to a low ACZ value, thus being the regions with the greatest negative changes. Notably, these regions include the inferior parietal lobe bilaterally which also overlap with the regional CBF reduction in the MCI group in the basal condition (Fig. 3.C).

Of interest is also the opposite change of C_{nodal} (increase) and SA_{nodal} (decrease) in the right middle frontal region (the top of the Fig. 6.E and the bottom of the Fig. 6.G, respectively), which partially corresponds with the regional CBF increase in the MCI group (Fig. 2.B).

As a final point, let us consider some issues regarding our study population of MCI patients. The criteria for patient selection and the episodic memory reduction in the MCI group (Supplementary Table S1) indicate that our patients presented amnestic MCI. Furthermore, hippocampal atrophy in the MCI group (Supplementary Fig. S3 and Supplementary Table S4) suggests that most of our patients could evolve to AD dementia, with an intermediate level of certainty according to the latest diagnostic criteria for MCI due to AD (Albert et al., 2011). Still, we cannot exclude the possibility that some of our MCI patients evolve to another type of degenerative dementia as MCI is a complex heterogeneous condition.

4.3. Study limitations

First, some results at the nodal level and their interpretations should be taken with caution since they are based on an uncorrected statistic. Yet, these findings are meaningful given the partial correspondence found with the other results in this study using a corrected statistic. In order to increase the effect size at the nodal level, it may be necessary to increase the number of subjects and/or to use a more potent vasodilator stimulus in future studies. Second, our results are only valid at the group level. However, the present study is a necessary first step for a further study based on individual level. A recent study demonstrated that it is possible to estimate the individual contribution of a single subject to group-based correlation networks and to examine its association with clinical data (Saggar et al., 2015). A third limitation

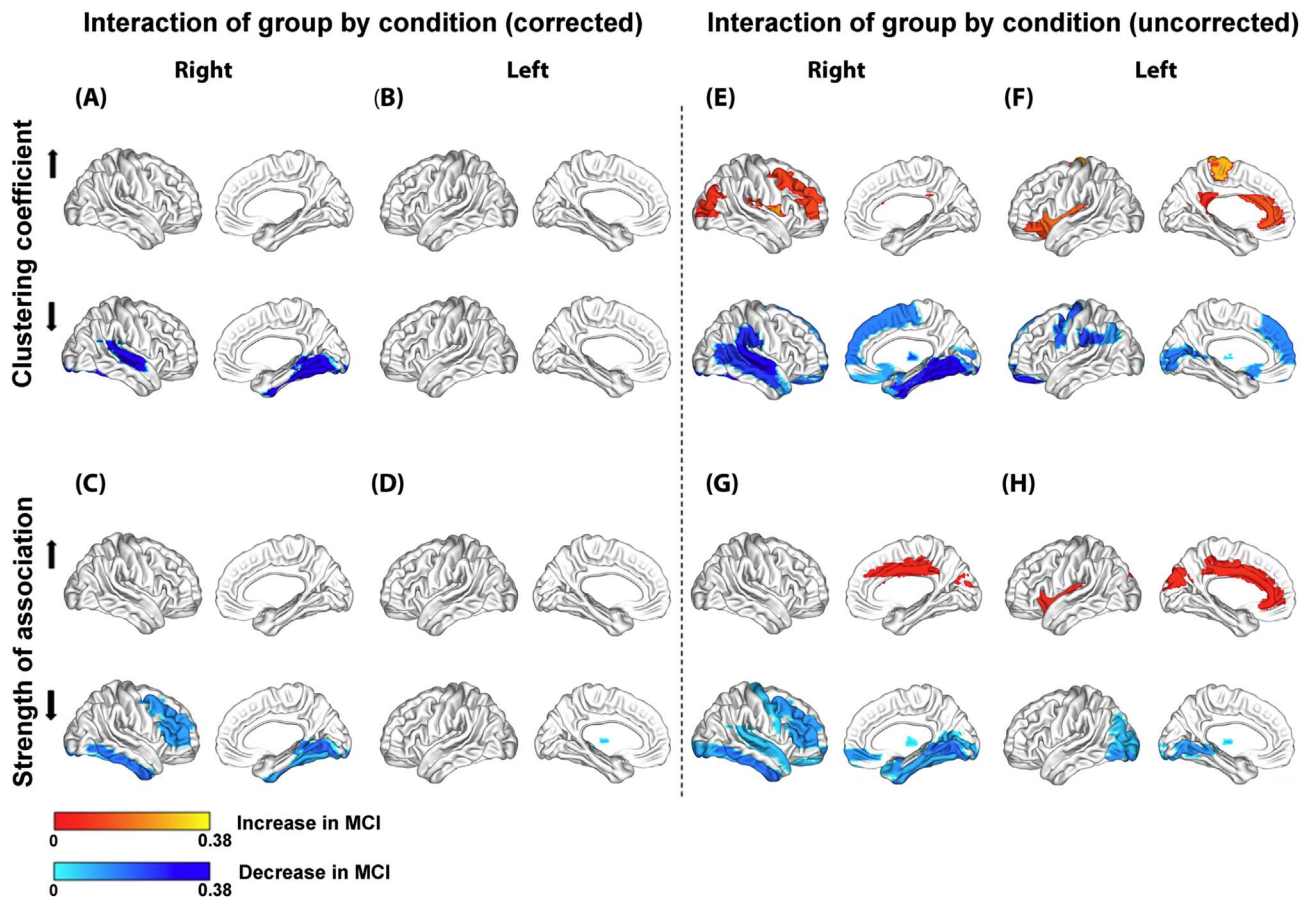

Fig. 6. Significant crossover interaction effects of group and condition at the nodal level for the clustering coefficient (C_{nodal}) and mean strength of association (SA_{nodal}) with Bonferroni correction (A–D) and without correction (E–H).
Regional changes are mapped onto the cortical surfaces using the BrainNet Viewer package (http://www.nitrc.org/projects/bnv).

is that this is a cross-sectional study, whereas longitudinal studies are needed to clarify the temporal evolution of the CBF_{corr} network along the continuum from normal aging to AD dementia. Four, graph theoretical analysis of the CBF_{corr} network has limitations that were discussed in our previous article (e.g. the use of Pearson's correlation instead of partial correlation; choice of parcellation scheme; possible variability of results with different sample sizes) (Melie-García et al., 2013). In addition, a recent study showed that the inclusion of global CBF as a confounding variable introduces artificial negative correlations in networks using resting state fMRI data (Carbonell et al., 2014), which might also be present in correlation networks using CBF SPECT. Nevertheless, all of these limitations are attenuated to some extent by studying the CBF_{corr} network in two different conditions, i.e. by analyzing the vasodilatory effect of ACZ after subtracting the effect of baseline. The vasodilatory effect of ACZ could be considered comparatively greater than the effects of the above methodological shortcomings.

4.4. Conclusions

This study suggests that graph theoretical analysis of ACZ-induced changes in the topology of the CBF_{corr} networks can detect subtle network-related CVR alterations in MCI not reflected by the standard approach. These alterations involve brain regions directly related to cognitive dysfunction in MCI. Our results also warrant further research on the individual level to develop a 'network'-based CVR biomarker of MCI due to AD.

Acknowledgements

The authors thank the collaboration of Drs. Yasser Iturria-Medina, Luis Juárez Orozco, Yurelis Ginarte and Fransje Reesink for their invaluable helps. The authors also thank the support of the Center for Neurological Restoration (CIREN), Havana, Cuba, and Department of Nuclear Medicine and Molecular Imaging, University Medical Center Groningen, the Netherlands.

Appendix A. Supplementary data

Supplementary data to this article can be found online at http://dx.doi.org/10.1016/j.nicl.2017.04.019.

References

Achard, S., Bullmore, E., 2007. Efficiency and cost of economical brain functional networks. PLoS Comput. Biol. 3 (2), e17.
Achard, S., Salvador, R., Whitcher, B., Suckling, J., Bullmore, E., 2006. A resilient, low frequency, small-world human brain functional network with highly connected association cortical hubs. J. Neurosci. 26 (1), 63–72.
Albert, M.S., DeKosky, S.T., Dickson, D., Dubois, B., Feldman, H.H., Fox, N.C., Gamst, A., Holtzman, D.M., Jagust, W.J., Petersen, R.C., Snyder, P.J., Carrillo, M.C., Thies, B., Phelps, C.H., 2011. The diagnosis of mild cognitive impairment due to Alzheimer's disease: recommendations from the National Institute on Aging-Alzheimer's Association workgroups on diagnostic guidelines for Alzheimer's disease. Alzheimers Dement. 7 (3), 270–279.
Alexander-Bloch, A., Giedd, J.N., Bullmore, E., 2013. Imaging structural co-variance between human brain regions. Nat. Rev. Neurosci. 14 (5), 322–336.
Anzola, G.P., Galluzzi, S., Mazzucco, S., Frisoni, G.B., 2011. Autonomic dysfunction in mild cognitive impairment: a transcranial Doppler study. Acta Neurol. Scand. 124 (6), 403–409.
Bassett, D.S., Nelson, B.G., Mueller, B.A., Camchong, J., Lim, K.O., 2012. Altered resting state complexity in schizophrenia. NeuroImage 59 (3), 2196–2207.

Boles Ponto, L.L., Schultz, S.K., Watkins, G.L., Hichwa, R.D., 2004. Technical issues in the determination of cerebrovascular reserve in elderly subjects using 15O-water PET imaging. NeuroImage 21 (1), 201–210.
Bullmore, E.T., Bassett, D.S., 2011. Brain graphs: graphical models of the human brain connectome. Annu. Rev. Clin. Psychol. 7, 113–140.
Cantin, S., Villien, M., Moreaud, O., Tropres, I., Keignart, S., Chipon, E., Le Bas, J.F., Warnking, J., Krainik, A., 2011. Impaired cerebral vasoreactivity to CO_2 in Alzheimer's disease using BOLD fMRI. NeuroImage 58 (2), 579–587.
Carbonell, F., Bellec, P., Shmuel, A., 2014. Quantification of the impact of a confounding variable on functional connectivity confirms anti-correlated networks in the resting-state. NeuroImage 86, 343–353.
Fromm, A., Lundervold, A.J., Moen, G., Skulstad, S., Thomassen, L., 2013. A vascular approach to mild amnestic cognitive impairment: a pilot study. Acta Neurol. Scand. Suppl. 196, 73–76.
Glodzik, L., Rusinek, H., Brys, M., Tsui, W.H., Switalski, R., Mosconi, L., Mistur, R., Pirraglia, E., de Santi, S., Li, Y., Goldowsky, A., de Leon, M.J., 2011. Framingham cardiovascular risk profile correlates with impaired hippocampal and cortical vasoreactivity to hypercapnia. J. Cereb. Blood Flow Metab. 31 (2), 671–679.
Glodzik, L., Randall, C., Rusinek, H., deLeon, M.J., 2013. Cerebrovascular reactivity to carbon dioxide in Alzheimer's disease. J. Alzheimers Dis. 35 (3), 427–440.
Hafkemeijer, A., van der Grond, J., Rombouts, S.A., 2012. Imaging the default mode network in aging and dementia. Biochim. Biophys. Acta 1822 (3), 431–441.
Hamilton, M., 1960. A rating scale for depression. J. Neurol. Neurosurg. Psychiatry 23, 56–62.
He, Y., Chen, Z.J., Evans, A.C., 2007. Small-world anatomical networks in the human brain revealed by cortical thickness from MRI. Cereb. Cortex 17 (10), 2407–2419.
He, Y., Chen, Z., Gong, G., Evans, A., 2009a. Neuronal networks in Alzheimer's disease. Neuroscientist 15 (4), 333–550.
He, Y., Dagher, A., Chen, Z., Charil, A., Zijdenbos, A., Worsley, K., Evans, A., 2009b. Impaired small-world efficiency in structural cortical networks in multiple sclerosis associated with white matter lesion load. Brain 132 (Pt 12), 3366–3379.
Herholz, K., Schopphoff, H., Schmidt, M., Mielke, R., Eschner, W., Scheidhauer, K., et al., 2002. Direct comparison of spatially normalized PET and SPECT scans in Alzheimer's disease. J. Nucl. Med. 43, 21–26.
Iadecola, C., 2004. Neurovascular regulation in the normal brain and in Alzheimer's disease. Nat. Rev. Neurosci. 5 (5), 347–360.
Ingelsson, M., Fukumoto, H., Newell, K.L., Growdon, J.H., Hedley-Whyte, E.T., Frosch, M.P., Albert, M.S., Hyman, B.T., Irizarry, M.C., 2004. Early Abeta accumulation and progressive synaptic loss, gliosis, and tangle formation in AD brain. Neurology 62 (6), 925–931.
Ingvar, D.H., 1979. “Hyperfrontal” distribution of the cerebral grey matter flow in resting wakefulness; on the functional anatomy of the conscious state. Acta Neurol. Scand. 60 (1), 12–25.
Iturria-Medina, Y., Sotero, R.C., Canales-Rodríguez, E.J., Alemán-Gómez, Y., Melie-García, L., 2008. Studying the human brain anatomical network via diffusion-weighted MRI and Graph Theory. NeuroImage 40 (3), 1064–1076.
Lassen, N.A., Andersen, A.R., Friberg, L., Paulson, O.B., 1988. The retention of [99mTc]-d,l-HM-PAO in the human brain after intracarotid bolus injection: a kinetic analysis. J. Cereb. Blood Flow Metab. 8 (6), S13–S22.
Melie-García, L., Sanabria-Diaz, G., Iturria-Medina, Y., Alemán-Gómez, Y., 2010. MorphoConnect: toolbox for studying structural brain networks using morphometric descriptors. In: 16th Annual Meeting of the Organization for Human Brain Mapping, (Barcelona, Spain).
Melie-García, L., Sanabria-Diaz, G., Sánchez-Catasús, C., 2013. Studying the topological organization of the cerebral blood flow fluctuations in resting state. NeuroImage 64, 173–184.
Morris, J.C., 1993. The clinical dementia rating (CDR): current version and scoring rules. Neurology 43 (11), 2412–2414.
Pillai, J.J., Mikulis, D.J., 2015. Cerebrovascular reactivity mapping: an evolving standard for clinical functional imaging. AJNR Am. J. Neuroradiol. 36 (1), 7–13.
Richiardi, J., Monsch, A.U., Haas, T., Barkhof, F., Van de Ville, D., Radü, E.W., Kressig, R.W., Haller, S., 2014. Altered cerebrovascular reactivity velocity in mild cognitive impairment and Alzheimer's disease. Neurobiol. Aging 36 (1), 33–41.
Rugg, M.D., Vilberg, K.L., 2013. Brain networks underlying episodic memory retrieval. Curr. Opin. Neurobiol. 23 (2), 255–260.
Saggar, M., Hosseini, S.M., Bruno, J.L., Quintin, E.M., Raman, M.M., Kesler, S.R., Reiss, A.L., 2015. Estimating individual contribution from group-based structural correlation networks. NeuroImage 120, 274–284.
Sanabria-Diaz, G., Martinez-Montes, E., Melie-Garcia, L., 2013. Glucose metabolism during resting state reveals abnormal brain networks organization in the Alzheimer's disease and mild cognitive impairment. PLoS ONE 8 (7), e68860.
Sánchez-Catasús, C.A., Stormezand, G.N., van Laar, P.J., De Deyn, P.P., Sánchez, M.A., Dierckx, R.A., 2017. FDG-PET for prediction of AD dementia in mild cognitive impairment. A review of the state of the art with particular emphasis on the comparison with other neuroimaging modalities (MRI and perfusion SPECT). Curr. Alzheimer Res. 14, 127–142.
Shim, Y., Yoon, B., Shim, D.S., Kim, W., An, J.Y., Yang, D.W., 2015. Cognitive correlates of cerebral vasoreactivity on transcranial Doppler in older adults. J. Stroke Cerebrovasc. Dis. 24 (6), 1262–1269.
Takasawa, M., Murase, K., Oku, N., Yoshikawa, T., Osaki, Y., Imaizumi, M., Matsuzawa, H., Fujino, K., Hashikawa, K., Kitagawa, K., Hori, M., Matsumoto, M., 2002. Assessment of acetazolamide reactivity in cerebral blood flow using spectral analysis and technetium-99m hexamethylpropylene amine oxime. J. Cereb. Blood Flow Metab. 22 (8), 1004–1009.
Tijms, B.M., Wink, A.M., de Haan, W., van der Flier, W.M., Stam, C.J., Scheltens, P., Barkhof, F., 2013. Alzheimer's disease: connecting findings from graph theoretic studies of brain networks. Neuorobiol. Aging 34 (8), 2023–2036.
Tzourio-Mazoyer, N., Landeau, B., Papathanassiou, D., Crivello, F., Etard, O., Delcroix, N., Mazoyer, B., Joliot, M., 2002. Automated anatomical labeling of activations in SPM using a macroscopic anatomical parcellation of the MNI MRI single-subject brain. NeuroImage 15 (1), 273–289.
Vagal, A.S., Leach, J.L., Fernandez-Ulloa, M., Zuccarello, M., 2009. The acetazolamide challenge: techniques and applications in the evaluation of chronic cerebral ischemia. AJNR Am. J. Neuroradiol. 30 (5), 876–884.
Van Laere, K.J., Versijpt, J., Koole, M., Vandenberghe, S., Lahorte, P., Lemahieu, I., Dierckx, R.A., 2002. Experimental performance assessment of SPM for SPECT neuroactivation studies using a subresolution sandwich phantom design. NeuroImage 16 (1), 200–216.
Villain, N., Chételat, G., Grassiot, B., Bourgeat, P., Jones, G., Ellis, K.A., Ames, D., Martins, R.N., Eustache, F., Salvado, O., Masters, C.L., Rowe, C.C., Villemagne, V.L., AIBL Research Group, 2012. Regional dynamics of amyloid-β deposition in healthy elderly, mild cognitive impairment and Alzheimer's disease: a voxelwise PiB-PET longitudinal study. Brain 135 (Pt 7), 2126–2139.
Watts, D.J., Strogatz, S.H., 1998. Collective dynamics of ‘small-world’ networks. Nature 393, 440–442.
Wu, K., Taki, Y., Sato, K., Kinomura, S., Goto, R., Okada, K., Kawashima, R., He, Y., Evans, A.C., Fukuda, H., 2012. Age-related changes in topological organization of structural brain networks in healthy individuals. Hum. Brain Mapp. 33 (3), 552–568.
Yamauchi, H., Okazawa, H., Kishibe, Y., Sugimoto, K., Takahashi, M., 2002. Reduced blood flow response to acetazolamide reflects pre-existing vasodilation and decreased oxygen metabolism in major cerebral arterial occlusive disease. Eur. J. Nucl. Med. Mol. Imaging 29 (10), 1349–1356.
Zavoreo, I., Kes, V.B., Morovic, S., Seric, V., Demarin, V., 2010. Breath holding index in detection of early cognitive decline. J. Neurol. Sci. 299 (1–2), 116–119.